Sedimentary Processes and Instability on the Mississippi River Delta Front near the Shipwreck of the SS Virginia

Nathan Figueredo *, Sam Bentley, Jason Chaytor, Kehui Xu, Navid Jafari, Ioannis Y. Georgiou, Melanie Damour, Jeffrey Duxbury, Jeffrey Obelcz, Jillian Maloney

Posted Date: 22 December 2023

doi: 10.20944/preprints202312.1742.v1

Keywords: Mississippi River Delta; Sediment Deposition; Fine-grained sediment transport; Sedimentary fabric; Sediment gravity flow; Slope Stability

Article

Sedimentary Processes and Instability on the Mississippi River Delta Front Near the Shipwreck of the Ss *Virginia*

Nathan Figueredo [1,*], Sam Bentley [1], Jason Chaytor [2], Kehui Xu [1], Navid Jafari [1], Ioannis Y. Georgiou [3], Melanie Damour [4], Jeffrey Duxbury [1], Jeffrey Obelcz [5] and Jillian Maloney [6]

[1] Louisiana State University; NF nfigue2@lsu.edu, SB sjb@lsu.edu, KX kxu@lsu.edu, NJ njafari@lsu.edu, JD Jeffrey.e.duxbury@gmail.com
[2] United States Geological Survey; jchaytor@usgs.gov
[3] The Water Institute; IG igeorgiou@thewaterinstitute.org
[4] Bureau of Ocean Energy Management; Melanie.Damour@boem.gov
[5] Naval Research Lab; jeffrey.obelcz@nrlssc.navy.mil
[6] San Diego State University; jmaloney@sdsu.edu
* Correspondence: nfigue2@lsu.edu

Abstract: Sediment cores were collected from a mudflow lobe (80 m water depth) offshore of the Mississippi River's Southwest Pass in 2017 to better understand the sedimentology near the lobe entraining the SS *Virginia* shipwreck (sunk by a German U-Boat in 1942) and surrounding Mississippi River Delta Front. Core analyses included ^{210}Pb/^{137}Cs geochronology, granulometry, and X-radiography. Sediment accumulation rates (SAR) calculated from excess ^{210}Pb activity in multicores are 0.22–0.29 cm/yr at seabed depths less than 20 cm and 0.29–0.51 cm/year at depths greater than 20 cm. ^{137}Cs accumulation rates are ~0.15 to ~ 0.37 cm/year since 1954 and 1963 respectively. Sediment accumulation rates from ^{210}Pb and ^{137}Cs geochronology and indicators of relative sedimentation and bioturbation from X-radiographs suggest that rates of sediment accumulation near *Virginia* have declined since ca. the mid-20th century. This may be explained by the multi-decade downslope mass transport of the mudflow lobe in which the shipwreck is embedded, and decreases in sediment supply delivered offshore from the Mississippi River. Mass-transport calculations of the *Virginia* lobe derived from core properties and published lobe advection rates suggest downslope mass transport is far higher than sediment resupply from the Mississippi River, consistent with recent studies of delta retreat.

Keywords: Mississippi River Delta; Sediment Deposition; Fine-grained sediment transport; Sedimentary fabric; Sediment gravity flow; Slope Stability

1. Introduction

1.1. Background

The Mississippi River Delta Front (MRDF) is an apron of sediment extending from approximately 5 m to 200 m water depth offshore of the southernmost distributaries of the Birdsfoot Delta of the Mississippi River. The MRDF is sculpted by mass wasting processes that produce its distinctly irregular seafloor morphology of collapse features, gullies, and lobes [1,2]. Recent research shows large sections of MRDF seabed have begun to retreat in the last decades after centuries of progradation [2–4]. At present, the cause of this retreat, whether by erosion, mass-transport of sediment further downslope, other processes, or a combination thereof, remains unknown. As part of a larger, multi-institutional study of the MRDF [5,6] funded by the Bureau of Ocean Energy Management (BOEM), this study employed geological and geochronological analysis of sediment cores to elucidate sedimentary processes active in one mudflow lobe of the MRDF that is the resting place of the WWII shipwreck SS *Virginia* [7]. The SS *Virginia* is a bulk oil tanker that sank on May 12, 1942, after being hit by three torpedoes from a German U-boat and is a war grave. It was discovered

 doi:10.20944/preprints202312.1742.v1

in 2001 during an oil and gas survey. The shipwreck is largely intact; its bow points to the northwest, and it lists to its port side in 80 m of water embedded within a mudflow lobe produced by mass transport off Southwest Pass [8].

1.2. Study area

This research primarily focused on *Virginia*'s location to the southeast of the Southwest Pass River outlet (Figures 1 and 2) on the MRDF. The shipwreck is embedded within a mudflow lobe with a 2-m-deep seafloor depression formed around the bow (Figure 2). The depression was present in 2017 but may be gone based on 2023 USGS survey data that are being processed for release as of late 2023 (Jason Chaytor, personal communication). The location of the shipwreck has been tracked in historical bathymetric surveys by Chaytor et al. (2020), documenting the shipwreck's movement as follows [8]. The shipwreck was originally discovered during a 2001 high-resolution geophysical survey for oil and gas-related operations and confirmed as *Virginia* in a 2004 remotely operated vehicle investigation. The shipwreck was later imaged ~365 m to the southeast during a post-Hurricane Katrina pipeline survey in 2005–2006. A 2009 geophysical survey reported that the shipwreck was located ~54 m southwest of its 2006 position while surveys in 2016 and 2017 showed another ~6 m of southwestern movement. In total ~430 m of movement occurred between 2001–2004 and 2017 with a -4.5 m relief change and no changes in orientation. Over the 75 years before the 2017 survey, *Virginia* has been displaced ~11 km downslope from where it reportedly sank. Regardless of possible inaccuracies in the reported sinking location, that initial location serves as a starting point for estimated movement. The shipwreck appears to be conjoined strongly to the mudflow lobe and any recent movements of the shipwreck probably involved movement of the entire mudflow lobe [8]. South of *Virginia* is the toe of the youngest mudflow lobe [8]. Approximate mudflow lobe boundaries are shown in Figure 2, encompassing an area approximately 2700m by 2700 m in extent.

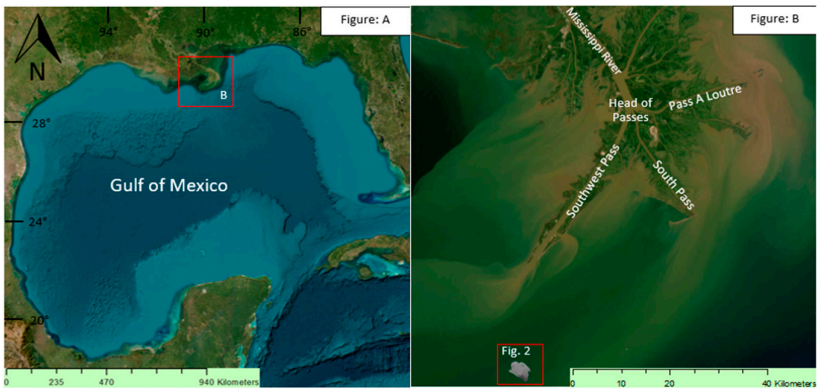

Figure 1. (A) Map of the Gulf of Mexico showing the location of the study area, 4B, within the gulf. (B) Map showing the bird's foot delta, within the Gulf of Mexico, highlighting the anatomy of the main distributary network.

Preprints (www.preprints.org) | NOT PEER-REVIEWED | Posted: 22 December 2023 doi:10.20944/preprints202312.1742.v1

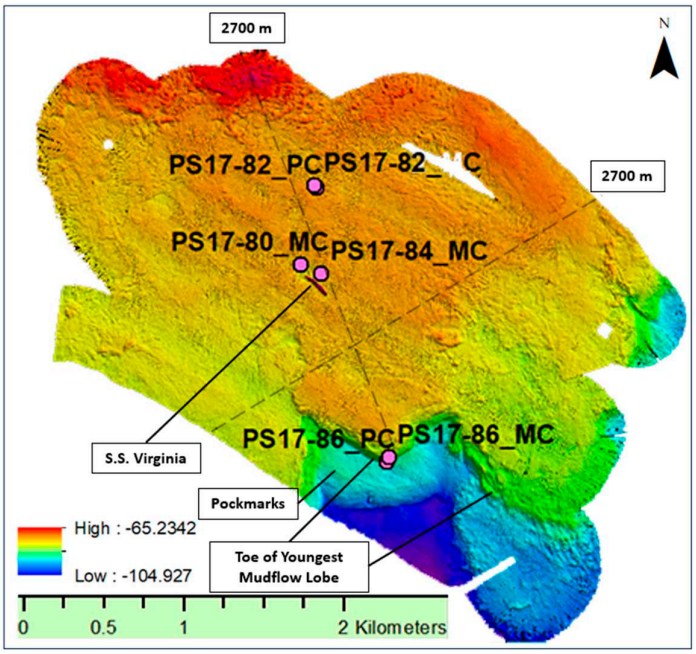

Figure 2. Depiction of the mudflow lobe adapted from Chaytor et al. (2020) in which the 153 m long SS *Virginia* is located pointing its bow towards the northwest. A depression is in lighter colors near the bow. There are no drag or scar features on the lobe, indicating that SS *Virginia* has been moving with the lobe rather than moving separately, across the lobe [8].

1.3. Hurricane influence

Hurricanes increase sediment entrainment from the seabed at the onset of larger waves and higher currents offshore the Mississippi River Delta [8]. Long-period waves associated with hurricanes can cause cyclic loading of the seabed that induces bottom shear stresses [1] resulting in sediment motion, including mass transport phenomena.

An example of the destructive capabilities of hurricane-induced mudflows is the Taylor Energy's production platform (MC20A) that was destroyed by a hurricane-induced mudflow during Hurricane Ivan (2004) resulting in substantial oil and gas release into the northern Gulf of Mexico as well as the dissolution of the Taylor Energy Company costing at least US $1 billion [9]. Guidroz (2009) conducted a risk assessment of hurricane-wave induced mudflows on the MRDF and identified the following criteria as necessary for producing waves strong enough to produce the largest mudflows: category 3 hurricane or larger, with slow transit across the MRDF region [10]. Hurricanes meeting these criteria since the onset of offshore oil and gas exploration in the 1950s and 1960s include Camille (1969), Ivan (2004), and Katrina (2005), each of which shifted large portions of MRDF mudflow lobes (including the *Virginia* lobe from at least hurricanes Ivan and Katrina), and damaged seabed infrastructure [10]. Findings in Obelcz et al. (2017), identified that lower intensity storms, such as cold fronts, also have the potential to produce failure or slides [11]. The continued tracking of *Virginia* and other nearby shipwrecks are important aspects of multi-component hazard vulnerability risk assessments, because of the cultural and historical importance of these sites (the National Historic Preservation Act of 1966 (54 USC § 306108)), and their utility as tracers for seabed motion.

1.4. Sediment Properties and the SS Virginia

Subaqueous sedimentary deposits of the Mississippi River Delta are controlled by seasonally and annually varying external inputs, such as river sediment delivery or storms, and quasi steady-state internal processes, such as sediment consolidation or biogenic gas production/release [2,8]. This study area is affected by multiple sediment dispersal processes including hypopycnal river plumes [12–14], storm wave/current induced resuspension [15–17], sediment slides driven by gravity acting

Preprints (www.preprints.org) | NOT PEER-REVIEWED | Posted: 22 December 2023 doi:10.20944/preprints202312.1742.v1

on a slope [11,18], and possibly also wave/current enhanced sediment gravity flows [19–21], although this type of flow has not yet been observed directly on the MRDF. The subaqueous delta is also now showing the effects of both recent (Allison et al., 2023) and long-term declines in sediment supply [4,22]. This change is manifested as the first-observed transgression of the subaqueous delta, indicated by the landward migration of 10-m isobaths near the three main historical river outlets, and upstream migration of substantial river discharge to new and expanding outlets upstream of the three major historic outlets (Figure 1) [3,22]. Interaction of these processes control the morphology and morphodynamics of the study area. In addition to historical and recent changes in sediment supply from the river [3,22], the downslope advection of the *Virginia* lobe should impact sediment accumulation rates on the lobe from the mid-20th century and later, by changing the local sediment supply and depositional setting of the *Virginia* sediment lobe, causing sediment accumulation rates (SARs) to decline over time due to both changing flux from the river, as well as changing depositional setting (due to lobe motion).

The rationale for this research is twofold: first, to better understand sediment-specific site formation processes near the shipwreck for the purposes of marine archaeological research, and second, to inform our understanding of the dynamics of sediment motion in the study area, forced by both hydrodynamic and gravity-driven phenomena. This is possible in part because the shipwreck's location can be used as a tracer of seabed movement [8].

2. Materials and Methods

2.1. Field Work and Core Processing

In June 2017, a U.S. Geological Survey (USGS) cruise on the R/V Point Sur conducted a high-resolution geophysical survey across the MRDF [8,23]. A second cruise in 2017 led by Louisiana State University (LSU) collected piston cores and multicores (Table 1) from specific depositional settings mapped by the USGS. Samples were collected using a Benthos piston corer (core diameter of 7.5 cm), capable of collecting cores up to 8 m depth in seabed, and an Ocean Instruments MC-800 multi-corer (core diameter of 10 cm), that collects sediment with limited disturbance up to 50 cm depth. Observations during core collection of all piston cores revealed evidence of gas expansion when processing cores on deck. Piston cores PS17-82-PC and PS17-86-PC were selected to provide data on opposing sides of the shipwreck site. Multi-cores PS17-80-MC and PS17-84-MC were selected due to their central positioning on the lobe as well as being ~80 m and ~50 m from *Virginia*. PS17-86-MC was added for comparison to its piston core PS17-86-PC to account for possible sediment non-recovery from the top 50 cm of the corresponding piston core. The positioning of the selected cores can be seen in Figure 2. Rectangular slabs were extracted from multicore tubes onboard the ship for subsequent imaging, and one multicore tube per deployment was extruded and sliced at 2-cm intervals for radiochemical and granulometric measurements with subsamples refrigerated in sealed plastic bags until analysis.

Table 1. Summary of collected piston and multi-cores.

Station	Distance from SW Pass (km)	Distance from SS *Virginia* (m)	Depth from Sea Level (m)	Penetration Depth (cm)
PS17-80-MC	18.99	150	84.7	18
PS17-82-MC	18.49	612	83.7	40
PS17-84-MC	19.03	69	84.3	28
PS17-86-MC	20.17	1174	88.8	34

Preprints (www.preprints.org) | NOT PEER-REVIEWED | Posted: 22 December 2023 doi:10.20944/preprints202312.1742.v1

PS17-82-PC	18.5	595	83.8	862
PS17-86-PC	20.14	1192	89	564

Cores were returned to LSU and kept in refrigeration pending analysis. Grain size distributions, sediment fabric, radionuclide distributions, and gamma density, were measured and interpreted in conjunction with the geophysical survey data from the 2017 USGS surveys to elucidate dominant sedimentary processes and their spatial and temporal patterns. Gamma density for piston cores was measured in July 2017 using a Geotek Multi Sensor Core Logger (MSCL) [23].

2.2. Sedimentological analyses

Granulometric analyses were conducted on samples extracted at 2-cm intervals from the cores using a Beckman-Coulter LS13-320 laser diffraction instrument following the methods of Restreppo et al. (2019) [24]. Core slabs for x-radiography sedimentary fabric analysis were imaged using a Samsung Model SP501 X-ray digital detector panel illuminated by a Min Xray HF-80 X-ray generator and evaluated for sedimentary fabric and macrostructures using the image processing program Image-J [19]. Split piston cores were imaged using an aluminum compensation plate machined to a parabolic profile to even exposure of the half-round slabs, refining an approach developed by Baker and Friedman (1969) for film-based radiography [25].

2.3. Radionuclide Analysis

Sediment was subsampled for granulometric and radiochemical analyses from multi-cores at 2-cm intervals, and every 12 cm for working halves of split piston cores. Intervals were selected to provide adequate resolution for dating without being too costly in detector time. The primary radionuclides of interest are excess ^{210}Pb (natural ^{238}U series, $t_{1/2}$ = 22.2 years) and ^{137}Cs (anthropogenic fallout, $t_{1/2}$ = 30.1 years). Data are reported in decays per minute per gram dry sediment (dpm/g), where 1 dpm=60 Bq.

Samples were dried and then ground using a mortar and pestle and sealed into petri dishes. Samples rested in sealed dishes for 14 days before ^{210}Pb data was collected, which allowed ingrowth of ^{210}Pb parent radionuclide ^{222}Rn and to determine supported activities. All samples were analyzed on Canberra BEGe 3825 detectors calibrated for energy and efficiency using standard reference materials with samples from a single core being restricted to one detector. ^{137}Cs was measured using the 661 keV peak for that radioisotope, with a detection limit of ~0.1 dpm/g. Sample self-absorption for ^{210}Pb gamma emissions were determined using the transmission method [26]. Activities associated with the 295 and 352 keV peaks of ^{214}Pb and the 609 keV peak of ^{214}Bi were averaged to determine the amount of supported ^{210}Pb. Supported ^{210}Pb activity is subtracted from total ^{210}Pb activity to determine excess ^{210}Pb activity.

For ^{137}Cs geochronology, we assume, based on Nittrouer et al. (1984): (1) ^{137}Cs was introduced into the environment in 1954 and was rapidly transferred to depositing sediments; (2) ^{137}Cs activities reached maximum values in the atmosphere in 1963; and (3) upon deposition, ^{137}Cs-laden sediments are rapidly mixed to the base of the bioturbated zone described as sediment deposits being disturbed by living organisms[27]. The accumulation rate based on ^{137}Cs can then be calculated from Equation 1:

$$A = (z_{max})\text{-}z_b)/\ (2017\text{-}(1963 \text{ or } 1954) \quad (1)$$

where A is the accumulation rate (cm/y), z_{max} is the depth of maximum ^{137}Cs (cm) for either 1954 (first appearance of ^{137}Cs) or 1963(peak activity of ^{137}Cs), z_b is the depth of bioturbation (cm), and 2017 is the year cores were collected [27].

Dominant processes that can influence the distribution of excess ^{210}Pb and other radionuclides in the shallow seabed include sedimentation (termed "advection" by Berner [1980])[28], radioactive decay, bioturbation, and erosion. An overall review of radiochemical and sedimentary fabric data

Preprints (www.preprints.org) | NOT PEER-REVIEWED | Posted: 22 December 2023 doi:10.20944/preprints202312.1742.v1

was used to determine the most logical combination of conditions when choosing equations. In settings where erosion depths are much less than thicknesses of sediment deposited, erosion is often ignored [29]. For ^{210}Pb geochronology, steady-state conditions are assumed, and rates of biturbation and sediment accumulation can be evaluated from Equations 2-4. For sediments containing excess ^{210}PB that are below the depth of bioturbation, long-term sedimentation rates (SAR) can be calculated from Equation 2 (adapted from Aller [1980] and Nittrouer and Sternberg [1981]) [29,30]. For conditions where bioturbation (represented as biodiffusion) and sediment accumulation are both important, Equation. 3 is used. For conditions where bioturbation and sediment accumulation are equally important in transporting sediments within the seabed, Eq. 4 is used.

$$A_z = A_0 \, e^{(-\lambda z/ws)} \quad (2)$$

$$A_z = A_0 \exp\left[(-z)/\sqrt{(D_b/\lambda)}\right] \quad (3)$$

$$A_z = A_0 \exp\left[z\cdot(w-\sqrt{(w^2-4D_b\lambda)})/(2D_b)\right] \quad (4)$$

where A_z is activity at depth z (dpm/g), A_0 is activity extrapolated to the sediment surface (dpm/g), λ is the decay constant of radionuclide of interest (y^{-1}), and S is the sediment accumulation rate (cm/y), and D_b is the biodiffusion coefficient (cm^2/y). Values for S, D_b, and A_0 were calculated using nonlinear least squares regressions after Muhammad et al. (2008) [31]. In addition, the age of the ^{210}Pb-laden deposit can be calculated by dividing the mean depth of the layer by the deposition rates obtained by Equation 4 [32].

Patterns of excess ^{210}Pb activity in sediment cores that suggest unsteady ^{210}Pb delivery (including multiple breaks in log-linear slopes, and undulatory profiles in log-linear plots) can indicate specific depositional processes. For example, fine sediment river plumes can deplete ^{210}Pb activity in marine waters, yielding sediment beds of fine grain size and low ^{210}Pb activity [32,33]. Sediment resuspension and deposition through storm activity and sediment gravity flows produces beds that fine upward and may contain stair-step patterns in ^{210}Pb activity. Bentley et al. (2002) found that horizontal "step treads" may represent erosional bed contacts and uniform riser activity may correspond with deposited beds wherein sediment has been homogenized, producing vertically uniform ^{210}Pb activities [35]. Additionally, variations in ^{210}Pb activity can be associated with grain size distribution with sands having lower ^{210}Pb activity than muds [32].

3. Results

3.1. Granulometry

Grain size volume frequency plots are shown for multi-cores in Figures 3–5 and piston cores in Figures 6 and 7. Overall, silt is the dominant grain size fraction, comprising ~70–90% of the samples. Granulometric data show a modal distribution in the very fine silt range (8–10 μm) indicated by warm colors in those plots. The clay sized material fraction content comprises 10–20% and sand content is 0–5%.

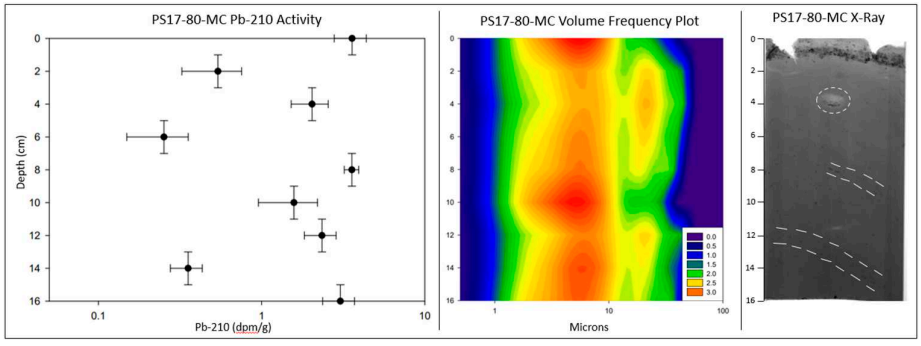

Figure 3. ^{210}Pb and ^{137}Cs profiles, grain-size frequency plot, and x-radiographic imaging of multi-core PS17-80-MC, immediately North of SS *Virginia*. X-radiographic images display higher density

Preprints (www.preprints.org) | NOT PEER-REVIEWED | Posted: 22 December 2023 doi:10.20944/preprints202312.1742.v1

sediment as darker gray shades, lower density sediment as lighter gray, and voids as white. The white dashed lines in the x-radiographic image highlights burrows outlined by iron flakes.

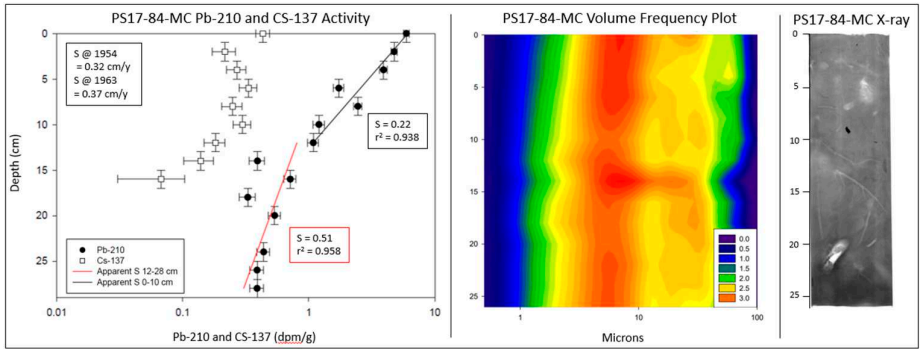

Figure 4. ^{210}Pb and ^{137}Cs profiles, grain-size frequency plot, and x-radiographic imaging of multi-core PS17-84-MC, East of SS *Virginia*. X-radiographic images display higher density sediment as darker gray shades, lower density sediment as lighter gray, and voids as white.

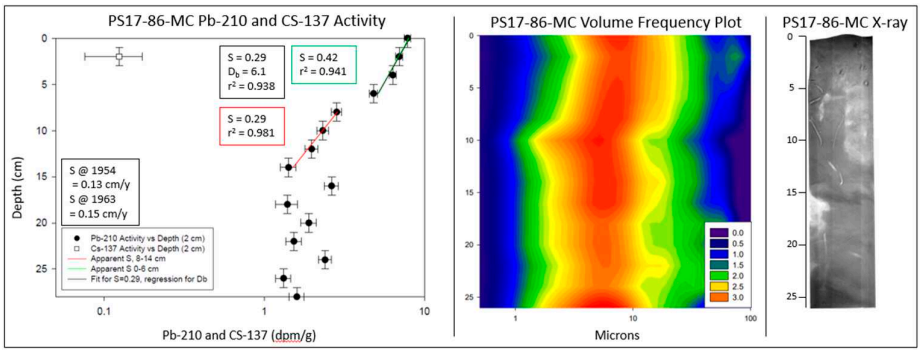

Figure 5. ^{210}Pb and ^{137}Cs profiles, grain-size frequency plot, and x-radiographic imaging of multi-core PS17-86-MC, at the toe of the mud lobe South of SS *Virginia*. X-radiographic images display higher density sediment as darker gray shades, lower density sediment as lighter gray, and voids as white.

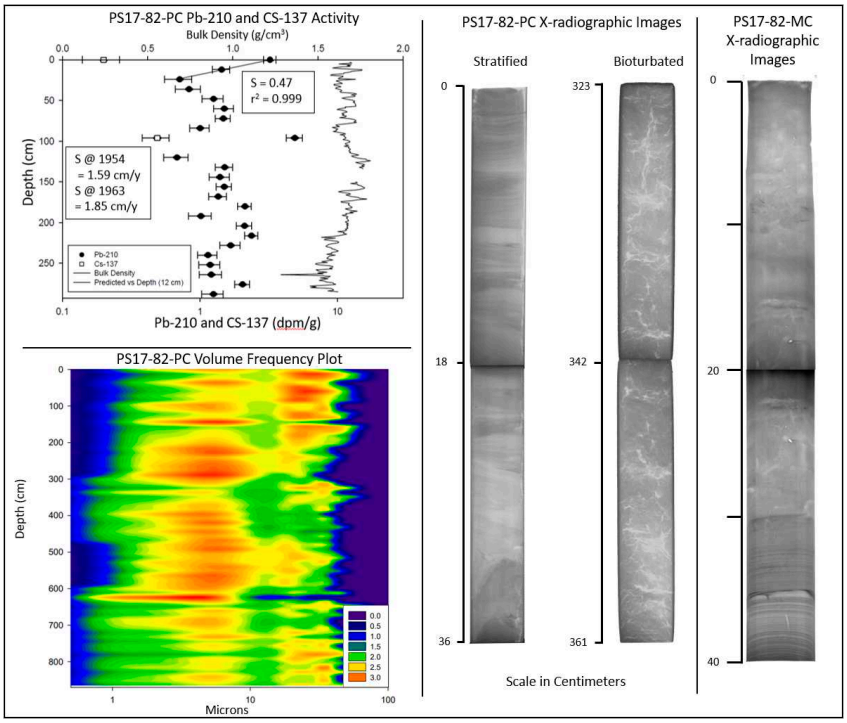

Preprints (www.preprints.org) | NOT PEER-REVIEWED | Posted: 22 December 2023 doi:10.20944/preprints202312.1742.v1

Figure 6. ^{210}Pb and ^{137}Cs profiles, grain-size frequency plot, and x-radiographic imaging of piston and multi-core PS17-82-PC, MC, at the Northmost portion of the mud lobe. X-radiographic images display higher density sediment as darker gray shades, lower density sediment as lighter gray, and voids as white.

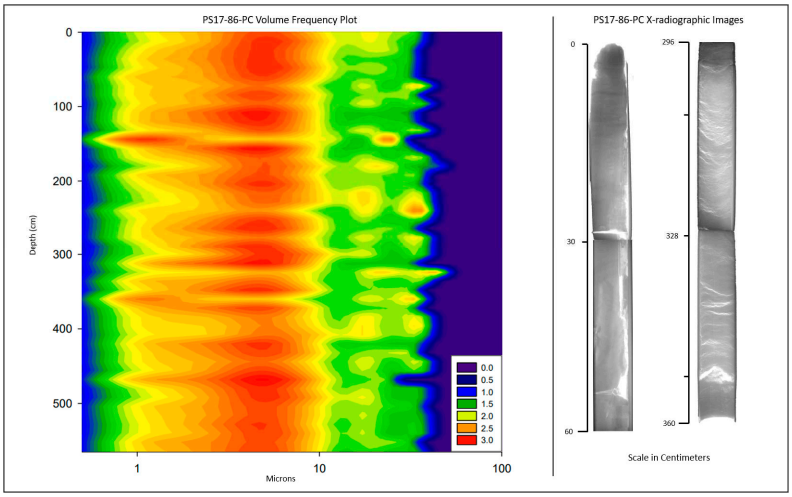

Figure 7. ^{210}Pb and ^{137}Cs profiles, grain-size frequency plot, and x-radiographic imaging of piston core PS17-86-PC, at the toe of the mud lobe. X-radiographic images display higher density sediment as darker gray shades, lower density sediment as lighter gray, and voids as white.

Multicores. PS17-80-MC (Figure 3) was collected ~80 m from the shipwreck (Figure 2). Sediment is fine-grained with generally homogenous grain size distribution, except for slight coarsening at 2–6 cm and 12–14 cm depth, associated with iron-oxide (rust) grains that are visible in the X-radiograph. PS17-84-MC (Figure 4) is generally homogenous excepting a slightly coarser zone near 14 cm depth. PS17-86-MC (Figure 5) coarsens slightly in modal grain size from bottom to top, from near ~7 μm at 25 cm depth to ~10 μm at the sediment-water interface.

Piston Cores. Piston cores in Figures 6 and 7 penetrated 5–8 m into the seabed and display much greater granulometric variability over these larger depth scales than do the short multicores. Both piston cores display generally bimodal variations downcore peaking at 101 μm in PS17-82-PC and 63 μm in PS17-86-PC (Figures 6 and 7).

3.2. X-Radiography

X-radiographs are scaled to display higher density sediment as darker gray shades, lower density sediment as lighter gray, and voids as white. Overall, X-radiographic images reveal four classes of sedimentary fabric and structures: biogenic mottling and biogenic sedimentary structures; stratified sediment layers that are likely the result of sediment deposition; inclined stratification; and light gray to white regions that are likely voids produced by biogenic gas expansion during core retrieval.

Multicores. PS17-80-MC (Figure 3) images show a stratified surface layer containing a layer of low-density sediments on top of iron oxide grains in the 0–2 cm depth interval, above mostly homogeneous sediment with a large, open burrow near 4 cm depth, and inclined burrows highlighted by iron oxide grains at 8–16 cm depth. PS17-82-MC (Figure 6) images show biogenic mottling and faintly stratified sediments in upper ~30 cm, underlain by less bioturbated and more stratified sediment at 30–40 cm depth; laminations and texture visible in X-radiographs in this interval appear like layering and grain texture to that of 0–15 cm depth in PS17-82-PC. PS17-84-MC (Figure 4) images show bioturbation with large, open, and partially filled outward facing and lengthwise burrows. Rust flakes (also identified during core subsampling for granulometry and radiochemistry) are also scattered throughout the core. PS17-86-MC (Figure 5) primarily shows

 doi:10.20944/preprints202312.1742.v1

bioturbation with faint physical stratigraphy near the bottom and lengthwise burrows. The faintly stratified lower section of the core is used as evidence for rapid muddy deposition.

Piston cores. Core PS17-82-PC was collected within ~100 m of multicore PS17-82-MC (Figure 2 and 6) and lacks the surficial zone of bioturbated sediments found in PS17-82-MC. This suggests PS17-82-PC did not recover the uppermost ~30 cm or more of the seabed. Deeper sediment displays faint cm-scale mottling and decimeter-scale variations in apparent density that may be remnant (unbioturbated) bedding. Below ~200 cm depth, arcuate sub horizontal voids likely created by gas expansion, observed during on-ship core processing, are evident to the base of the core at 825 cm. PS17-86-PC (Figure 7) shows faintly stratified sediments in the top 15 cm of the core. From 15 cm to the base of the core, cm-scale mottling and faintly bedded light-to-dark gray regions are apparent. Below ~200 cm depth, arcuate subhorizontal voids created by gas expansion occur to the base of the core at 394 cm depth.

3.3. Radionuclide analysis

Multicores. PS17-80-MC activity shows heterogenous vertical ^{210}Pb (0–16 cm) distribution and no obvious trends with depth (Figure 3), and ^{137}Cs is not detectable. No estimates of bioturbation or sediment accumulation are possible with these data using Equations 2-4 due to short core length and lack of a useful gradient or trend in the ^{210}Pb profile (required for application of equations 2-4).

PS17-84-MC activity has two separate gradients of ^{210}Pb activity versus depth that can be identified (Figure 4). Over 0–12 cm depth, an irregular log-linear gradient declines from the sediment-water interface. Over 12–25 cm, a variable and more vertical log-linear gradient is evident. If a regression for sedimentation and decay is applied (Eq. 2), accumulation rates are 0.22 cm/y over 0–12 cm and 0.51 cm /yr deeper in the core. However, given the mottling evident in the x-radiograph for this core, it is likely bioturbation also influences the ^{210}Pb gradient over 0–12 cm. If so, then the actual ^{210}Pb sediment accumulation rate is likely to be slower to account for the mixing effects of bioturbation. A well-defined ^{137}Cs profile is evident with ^{137}Cs first occurring at 16 cm depth, with a subsurface maximum at 8 cm depth. From Equation 1, accumulation from ^{137}Cs is 0.32 cm/yr since 1954, assuming a depth of rapid bioturbation of ~6 cm (estimated below). When rates are calculated from the peak value of ^{137}Cs that is assumed to represent ca. 1963, the ^{137}Cs sediment accumulation rate since 1963 is 0.37 cm/y.

PS17-86-MC shows three distinct zones of excess ^{210}Pb; ^{137}Cs is detectable only in one sample at 4 cm depth (Figure 5). The ^{210}Pb activity over 0–6 cm depth shows a steep sub-vertical log-linear decline. At 8–14 cm, a regular but less vertical decline is evident, below which the profile is vertical and irregular. The uppermost two zones define a profile consistent with marine-sedimentary ^{210}Pb analyses [30], influenced by mostly bioturbation in the upper zone, and mostly sediment accumulation in the lower zone, with radioactive decay active throughout. For regression analysis, the middle zone of the ^{210}Pb profile yields a sediment accumulation rate of 0.29 cm/y for 8–14 cm (Eq. 2). Using this value for sediment accumulation in a regression of Eq. 4 over the 0–6 cm zone yields $D_b \approx 6$ cm2/y (Table 2). The irregular vertical basal profile of excess ^{210}Pb suggests rapid deposition or mixing in this interval [35]. If the 0–6 cm were SAR only, the SAR only regression (Equation 2) would be 0.42 cm/y. The presence of a single detection of ^{137}Cs at 4 cm is difficult to assess. Two possibilities include earliest introduction (1954) or peak value (1963). If it were the first introduction, then sediment rates based on ^{137}Cs since 1954 would be 0.13 cm/y or less, depending on effects of bioturbation. If it were the peak value, then sediment rates based on ^{137}Cs since 1963 would be 0.15 cm/y or less, depending on effects of bioturbation.

Preprints (www.preprints.org) | NOT PEER-REVIEWED | Posted: 22 December 2023 doi:10.20944/preprints202312.1742.v1

Table 2. Summary of Radionuclide Regression Analysis.

Station	^{210}Pb SAR (cm/y)	r_2	^{210}Pb Depth Range (cm)	^{210}Pb SAR (cm/y)	r_2	^{210}Pb Depth Range (cm)	D_b	r_2	D_b Depth Range (cm)	^{137}Cs SAR 1954 (cm/y)	^{137}Cs Depth Range (cm/y)	^{137}Cs SAR 1963 (cm/y)	^{137}Cs Depth Range (cm/y)
PS17-84-MC	0.22	0.938	0-12	0.51	0.433	12-25	N/A	N/A	N/A	0.32	0-16	0.37	0-8
PS17-86-MC	0.42	0.981	0-6	0.29	0.981	8-14	6.1	0.938	0-6	0.13	0-4	0.15	0-4
PS17-82-PC	0.47	0.999	0-24	N/A	N/A	N/A	N/A	N/A	N/A	1.59	0-96	1.85	0-96

Piston cores. In PS17-82-PC excess ^{210}Pb is present over 0–200 cm, with a rapid decline with increasing depth over 0–24 cm, and a highly irregular but overall approximately vertical profile below 24 cm. ^{137}Cs is present at 0 and 96 cm (and may be present at other depths but below detection limits of ~0.1 dpm/g). Because this depth interval is unbioturbated, a regression using Eq. 2 (sediment accumulation and decay) for ^{210}Pb is appropriate and yields an SAR of 0.47 cm/y for 0–24 cm. It is uncertain whether the ^{137}Cs detected at 96 cm is closer to the first introduction or the peak value. If it were the first introduction, then sediment rates based on ^{137}Cs since 1954 would be 1.59 cm/y. If it were the peak value, then sediment rates based on ^{137}Cs since 1963 would be 1.85 cm/y. However, the two detections of ^{137}Cs over 96 cm provide few reference points for SAR estimation.

PS17-86-PC does not contain any excess ^{210}Pb or detectable ^{137}Cs, suggesting the uppermost tens of cm of sediment were either not recovered in the piston core, or were removed from the seabed by physical processes prior to coring.

3.4. Piston Core Density

Both piston cores show cm-scale and m-scale variations in density downcore, over density ranges of 0.1 g/cc for cm-scale variations and 0.4 g/cc for m-scale variations (Figure 8).

Preprints (www.preprints.org) | NOT PEER-REVIEWED | Posted: 22 December 2023 doi:10.20944/preprints202312.1742.v1

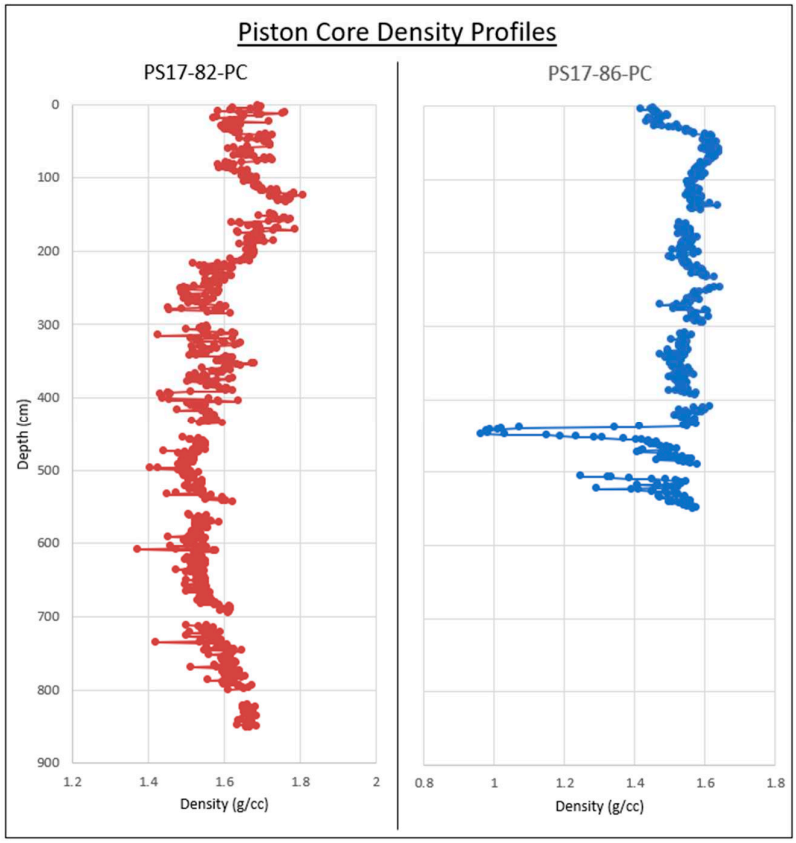

Figure 8. Density profiles of piston cores PS17-82 and PS17-86 at respective depths. Artifacts in density measurements created by open voids were removed. .

PS17-82-PC displays sawtooth variations of ~0.1–0.2 g/cc occur at the centimeter scale at 4–24 cm and 40–81 cm. A gradual downward increase occurs over 88–134 cm, below which density declines with variations downward from ~1.75 g/cc at 150 cm depth to ~1.6 g/cc at 250–400 cm depth. From 400 to ~675 cm depth, density varies around ~1.55 g/cc, then increases slowly to the base of the core, at ~1.65 g/cc.

PS17-86-PC's density increases sharply over 28–38 cm by ~0.3 g/cc. A slight density decreases of ~0.03 g/cc occurs at 41–79 cm, then varies in the range of 1.5–1.6 g/cc from 100 to 200 cm depth. Density then increases slightly to ~1.65 g/cc at 250 cm depth, then declines downward to ~1.55 g/cc over the 325–425 cm depth range.

4. Discussion

4.1. Rates and Distances of Lobe Motion

The movement of *Virginia* and its associated sediment lobe constitute one of the few multi-year and unambiguous records of large-scale, gravity-driven mass transport on the MRDF. Its historical movement over a 75-year period—especially the last two decades—highlights that both slow and rapid movement can occur [8]. Movement of the shipwreck is assumed to track that of the surrounding mudflow lobe because the two appear to be conjoined. If the reported 1942 sinking location is the approximate point the vessel came to rest on the seafloor and excluding undocumented hurricane-induced motion, the shipwreck site would have moved at an average rate of 147 m/y. This rate is nearly double the 2009–2016 rate of 85 m/y but is close to the Southwest Pass mudflow gully maximum measured displacement of 141 m over a two-month period for sediment blocks in mudflow gullies east of Southwest Pass [8,36]. From 2004 to 2017, the rate of motion was 30.7 m/y, becoming stationary during 2016–2017.

 doi:10.20944/preprints202312.1742.v1

Guidroz (2009) synthesized and analyzed observations for the movement of large MRDF sediment lobes due to the cyclic loading of the MRDF seabed by major hurricane waves [10]. Guidroz's (2009) analysis suggests that the substantial increases in lobe movement rate during periods of intense hurricane activity (2004–2006 and 2007–2009) are likely caused directly by hurricane activity and suggest that instantaneous rates (that have not yet been measured) might be even more rapid than the time-averaged displacement rates of Chaytor et al. (2020) [8,10]. This motion over 75 years appears to have transferred the shipwreck and sediment lobe from a location near the river outlet (with associated high SARs of 1.3–7.9 cm/y; Keller et al., 2016) to a region farther from the river outlet, where present SARs appear to be generally lower (Table 2) [32].

4.2. Radioisotope Geochronology and Sedimentary Fabric

Results of core analysis near *Virginia* exhibit some consistent trends among cores. Radionuclide data of multi-cores PS17-84-MC and PS17-86-MC both show historically faster sediment accumulation overlain by slower recent sediment accumulation and pervasive near-surface bioturbation in the vicinity of the shipwreck. PS17-80-MC is a short core that is not suitable for ^{210}Pb geochronology and does not reach the sediment-depth ranges of historical rapid sedimentation in other cores. However, it does exhibit signs of bioturbation in shallow sediments in X-radiographic images, suggesting slow sedimentation overprinted by bioturbation within the short depth of the core (like surface sediments in other multicores) [37]. For PS17-84-MC and PS17-86-MC, the bioturbation terms incorporated into the radionuclide regression analysis (represented as biodiffusion coefficient D_b and the apparent mixing depth L_b) are consistent with X-radiographic imaging showing evidence of bioturbation especially in the shallowest sediments. Each core contains two or more zones characterized by downward changes in ^{210}Pb gradients, which represent shifts from high SARs likely near and before ca. 1953 (when ^{137}Cs first appears in marine sediments globally). The top section of PS17-82-PC and PS17-82-MC show consistency with the other multi-cores suggesting steady sedimentation overlain by bioturbation. For PS17-82-PC below~24 cm, no SAR can be determined using equations 2-4; however, such irregular near-vertical profiles of excess ^{210}Pb have been associated with periods or events of rapid sediment deposition [35]. Where evidence for steady sedimentation is present, SARs range 0.42–0.51 cm/y. PS17-84-MC has the most complete ^{137}Cs profile. This allows for identification of first appearance at ~16 cm and peak activity at ~6 cm. Based on first appearance; sedimentation rates based on ^{137}Cs profile is 0.32 cm/y. This is consistent with sedimentation rate calculations based on ^{210}Pb activity (Table 2, Figure 3–5).

Sedimentary fabric in X-radiographic images shows fabric similarities among multicores, supporting the ^{210}Pb regression analysis. Multi-cores PS17-80-MC and PS17-84-MC are extensively bioturbated through the shallowest 12 cm, consistent throughout all cores for which the sediment-water interface was likely recovered. PS17-82-MC and PS17-86-MC show bioturbation near the surface as well as fully/partially stratified sections buried beneath. This is generally consistent with what is seen in the piston core sedimentary fabric and geochronology described for PS17-82-PC and PS17-86-PC. For instance, PS17-82-PC continues the stratification that is seen in the lower portion of its multi-core counterpart. PS17-86-PC shows similar results; however, its stratification is much fainter and potentially partially bioturbated in the multi-core.

PS17-80-MC is located within the depression at the bow of the shipwreck. This depression could be a current scour near the ship that hinders deposition and accumulation, potentially explaining its shallow penetration depth, short/irregular vertical ^{210}Pb profile and no detectable ^{137}Cs. Collectively, this could be explained by erosion and bypass of both historically ^{137}Cs-laden sediments as well as freshly deposited sediments with naturally elevated excess ^{210}Pb activities.

Downcore changes in apparent SAR and the vertical patterns of bioturbation (highest near the sediment surface) and stratification in core X-radiographs (generally more stratified towards the base of cores) together suggest that sediment delivery to the *Virginia* lobe may have declined over the last century. The presence of stratified sediment in multicores PS17-82 and PS17-86 below the 34 cm depth horizon suggests a recent relative increase in the degree of bioturbation in the sedimentary fabric. Bioturbating invertebrates in many subaqueous deltas are adapted to highly variable sediment

 doi:10.20944/preprints202312.1742.v1

deposition; therefore, rapid sedimentation is unlikely to disrupt this bioturbation [38,39]. A more likely explanation for this change from stratified fabric (least recent) to bioturbated sediment (most recent) is a reduction of sediment supply, which would allow for bioturbation acting at the same rate to produce more pervasive mixing of sediments before bioturbated sediments are buried below the depth of bioturbation [37]. This reasoning is also consistent with the observation of apparent downcore increases in SAR in cores PS17-84-MC and PS17-86-MC.

Downward increases in stratification and downcore reduction in apparent degree of bioturbation in both piston and multi-cores suggest that either the sediment supply to the region is declining, less deposited sediment is accumulating, the activities of bioturbating organisms are changing, or all the above. Although no time-series observations of bioturbation or benthic fauna are available, radioisotope geochronology combined with fabric analyses suggest that declining sediment supply and/or accumulation are a more robust explanation than changing bioturbation intensity. Results here suggest that the overall declining sediment accumulation began during the mid-20th century, which agrees with findings in [40].

Geochronology analyses presented here near *Virginia* contrast with previous studies done at sites within the MRDF region, using identical methods. In Duxbury et al., (2021), SARs were calculated at sites directly off Southwest Pass (water 30–80 m deep) and in deeper water (150–275 m) south of South Pass [41]. The ^{210}Pb SARs at Southwest Pass ranged 4.2–12.8 cm/y and at South Pass ranged 0.8–5.7 cm/y [41]. The ^{137}Cs values at Southwest Pass ranged 2.7–9.4 cm/y and at South Pass ranged 0.4–6.5 cm/y [41]. Keller et al. (2016) reported similar SAR results with cores taken ~7–12 km from Southwest Pass where ^{210}Pb SARs ranged 1.3–5.3 cm/y with one station reaching 40.7 cm/y [32]. Values found in Duxbury et al. (2023) and Keller et al. (2016) are substantially greater than those found around *Virginia*, where ^{210}Pb SARs ranged 0.22–0.47 cm/y and 0.29–0.51 cm/y downcore. In the case of Duxbury et al. (2023), where values are ~90% higher than those found at *Virginia*, core collection occurred over the same time frame, in similar seafloor morphology, and span both deeper and shallower water depths in locations off South Pass that fall at approximately the same distance from Southwest Pass [41]. A similar trend is present in ^{137}Cs accumulation rates, where Duxbury et al. (2023) calculations exceed those at *Virginia*, ~0.13 cm/y (this study)–1.59 cm/y (Duxbury et al., 2023) by ~90% [41].

4.3. Sediment Resuspension Potential from Combined Waves and Currents

Spatially, the greater MRDF is showing declining sediment accumulation across multiple locations. Sediment resuspension and non-deposition of sediment in transport is one possible explanation for the results above, if the present location of the *Virginia* lobe experiences higher bed-shear stresses than the locations of other nearby studies with higher SARs, and if the lobe has moved from a region of higher SARs to a region of lower SARs. This explanation would require that local wave-current bed-shear stresses are sufficient to resuspend deposited Mississippi River sediment plumes or prevent their initial deposition. Lo et al. (2016) and Sha et al. (2018) determined that shear stresses of 0.2–0.45 Pa are required to resuspend Mississippi River sediments that have been deposited (and experiencing consolidation) for 15–90 days, suggesting that lower shear stresses could prevent such sediments from depositing [42,43]. Xu et al. (2014) and Xu et al. (2011) used slightly lower shear stresses of 0.11 – 0.13 Pa on the shelf and in deeper canyons in their regional models of sediment transport that included the MRDF [44,45]. We are not aware of any benthic hydrodynamic or sediment-transport studies conducted in the region, including studies cited in Maloney et al.'s (2020) extensive review of MRDF sedimentary processes, so no direct measurements of local shear stresses appear to be available [2].

Results from Zang et al. (2019) numerical modeling study of sediment dynamics in the northern Gulf of Mexico from 1993 to 2012 include our study area and show that benthic hydrodynamic sedimentary processes on the MRDF are spatially and temporally heterogeneous and suggest that the downslope motion of the *Virginia* lobe could possibly influence sediment deposition and thus SARs on the lobe [46]. Zang et al. (2019, Figure 10) found a zone on the MRDF of elevated average bed-shear stresses of ~0.1 Pa from currents that focus between and parallel to the 50 and 200 m

Preprints (www.preprints.org) | NOT PEER-REVIEWED | Posted: 22 December 2023 doi:10.20944/preprints202312.1742.v1

isobaths year-round [46]. Figueredo (2022) studied a 2016–2017 time-series of ocean waves from nearby NOAA buoy 42040 and estimated that peak wave-generated shear stresses on the *Virginia* lobe reached 0.04 Pa for one winter storm, and 0.08 Pa during one tropical storm (no hurricanes impacted the area during this period). The total shear stress acting upon the seabed under wave and currents is greater than that predicted by simple linear addition of wave and current shear stresses [14]. Linear addition above yields combined wave-current shear stress of 0.14–0.18 Pa, suggesting that seabed resuspension is likely over annual timescales, and likely more intense under hurricanes. These findings suggest that sediment resuspension and bypass are likely at the *Virginia* lobe, at least for parts of the year.

Zang et al. (2019) also evaluated average seasonal sedimentation rates and lateral sediment fluxes through their models [46]. Near our study area, they found that fall and winter conditions are non-depositional despite elevated lateral sediment flux across the study area. In contrast, spring and summer conditions have high sediment flux, moderate sediment deposition (spring), and zero-to-low sediment deposition in summer. This combination of observations for sedimentation in our study area suggests that local heterogeneity of sediment supply and seabed hydrodynamics probably produces great heterogeneity in sediment bypass, resuspension, and accumulation, consistent with the hypothesis that downslope advection of the *Virginia* lobe (into a location of possibly stronger sediment resuspension/bypass) combined with historical decline in sediment supply have altered the local depositional environment, yielding a decline in SARs over the last ~50 years. However, these collected results are not yet conclusive for evaluating this hypothesis.

4.4. Estimating Total Gravity-Driven Mass Transport of the SS Virginia Sediment Lobe

Using bathymetric data and dimensions (Figure 2) and time-series estimates for the location of the *Virginia* shipwreck and sediment properties from core data [8], it is possible to estimate: the local volume of the *Virginia* lobe, speed of motion for the lobe, total dry mass of sediment in that volume moving downslope, and rate of mass transport for different periods. The volume of the mudflow lobe was estimated using Equation 5:

$$v = L \cdot W \cdot z \quad (5)$$

$$\text{Dry mass} = v \cdot (1-\varepsilon) \cdot 2.65 \quad (6)$$

where L is length, W is width, z is depth in meters, ε is porosity of bed, and 2.65 is the grain density in metric tons per m^3. Equation 7, from Whitehouse et al. (2000) was used to convert from bulk density to porosity [47]:

$$p_B = p + C_M ((p_s-p)/p_s) \quad (7)$$

where p_B is the density of water, excluding sediment, p is pressure (we define p=0, because fluid and sediment are incompressible at these depths), ps is the density of sediment grains, and C_M is the mass concentration (dry density) of sediment (mass/volume). Fractional porosity and bulk density were estimated from gamma-density measurements for basal portions of sediment cores (Figure 8). Mudflows triggered by hurricane waves have been identified as the potential causes for continuous movement of *Virginia* from 2004 to 2008, occurring in short pulses of apparently rapid movement [8]. If these motions record the advection of the entire sediment lobe as suggested by Chaytor et al. (2020), then a sediment volume likely greater than ~4 km^2 by >10 m thick (> 40,000,000 m^3) is placed in motion by these events (approximate dimensions in Figure 2) [8]. For simplicity, Equation 5 assumes the mudflow lobe is rectangular with dimensions of 2700 x 2700 m, which were measured across bathymetric data (Figure 2). The exact thickness for the action portion of the mudflow lobe is unknown; however, an approximate depth of ~16 m can be determined from bathymetric data (Figure 2). Because we do not know if the entire lobe moves or just a portion, depth intervals of 100%, 50%, and 10% of 16 m will be used for the lobe height estimate. Under these conditions, the volume of the mudflow in motion is estimated to be 117 x 10^6, 58.7 x 10^6, and 19 x 10^6 m^3 for the 100%, 50%, 10% height estimates, respectively. From these values, Equation 7 was used to calculate the dry sediment mass of the mudflow lobe, yielding 124 x 10^6, 62 x 10^6, and 20 x 10^6 metric tons. When compared to the estimated annual sediment load of the Mississippi River, 210 x 10^6 tons per year of which only 93.3 x 10^6 metric tons/y make it to Baton Rouge (upstream of diversions and outlets on the lower river

Preprints (www.preprints.org) | NOT PEER-REVIEWED | Posted: 22 December 2023 doi:10.20944/preprints202312.1742.v1

[48]; the dry mass values are approximately 133%, 62%, and 20% of the total yearly sediment load. Table 3 shows estimated total rates of sediment transport for the different active zone thicknesses to be 18–23,000 Mt/y depending on the slab thickness, and the speeds of motion, estimated from Figure 2. The time required to displace 100% of the lobe volume at the three different speeds of lobe motion is ≥15 years. The time required to displace the volume equivalent for one year of sediment load at Baton Rouge (through a frontal area like that of the *Virginia* lobe) is ≥7 years. Finally, the time required to displace the volume equivalent for one year of sediment load at Baton Rouge across the entire MRDF, assuming a lobe width of 2.7 km and MRDF width of 100 km is 0.03–0.12 years, at the rates of motion calculated from Figure 2.

Table 3. Mudflow Lobe Volume Analysis and Transport Rates.

Depth Interval (m)	Lobe volume undergoing transport (x 10^6 m3)	Dry Mass (x 10^6 metric tons per m3)	Percentage of Annual Sediment Load at Baton Rouge	Mass Transport Rate 2004-2006, Mt/y, using speed of 183 m/y (Figure 7), across full width of lobe	Transport Rate 2006-2009, t/y, using speed of 54 m/y (Figure 7), across full width of lobe	Mass Transport Rate 2009-2016, Mt/y using speed of 0.9 m/y (Figure 7), across full width of lobe
16	120	120	130	22,000	2,200	108
8	59	62	66	11,000	1,100	56
2.6	19	20	22	4,000	360	18

The amount of sediment exiting the main outlets of the Birdsfoot Delta at Southwest and South Passes and Pass a Loutre is not currently well-defined. Based on Allison et al. (2023), the present sediment discharge is on the order of 45% of the suspended load presently passing New Orleans [22]. If the mass transport velocities for the *Virginia* lobe are extrapolated across the entire MRDF, then at least parts of the MRDF are being depleted of sediments by mudflow activity faster than they can be resupplied by sediments delivered from the main river outlets below the Head of Passes. Assuming sediment accumulation is a major preconditioning or triggering factor, this suggests mudflow risk could decline in the future due to decreasing sediment accumulation on the MRDF and continued MRDF sediment depletion from mudflows.

Despite this, infrastructure on the seabed of the Gulf of Mexico is still in danger from mass movement events, especially infrastructure present in greater depths where flows that deplete sediment will continue to occur even if sediment accumulation continues to decline. The *Virginia* lobe currently lies 12 km upslope of eight pipelines [49]. On its current southwestern trajectory, the *Virginia* lobe will intersect a pipeline in ~5 km and seven more pipelines over ~12 km. Based on the transit time to evacuate the full lobe volume past the present front of the lobe (Table 4), *Virginia* could overtake the pipelines in ≥28 years on its current trajectory. This would pose substantial environmental and economic risk if the pipelines and platforms are still in operation.

Table 4. Mudflow Lobe Speed and Transit Time.

Speed of Flow (m/y)	Transit Time (y) to Evacuate Full Lobe Volume Past the Present Front of the Lobe	Transit Time (y) for a Volume Equivalent to one Year Sediment Load at Baton Rouge	Transit Time (y) for a year-equivalent Discharge Volume Across Entire Delta Front (if front is 100 km across, and lobe width is 2 km)
183	15	12	0.06
54	50	40	0.2
0.9	2985	2407	12

5. Conclusions

This study focuses on the WWII shipwreck SS *Virginia* and the underlying sediment lobe on the MRDF. Specifically, signs of recent deposition, mass failure, and overall migration of the shipwreck were examined. Analysis of sediment cores and geophysical data for the lobe beneath the shipwreck

allowed a multifaceted approach to exploring sediment dynamics of the area. The major findings can be summarized as follows:

1. Sediment accumulation rates from ^{210}Pb and ^{137}Cs geochronology as well as relative indicators of sedimentation and bioturbation ascertained from core X-radiographs suggest that rates of sediment accumulation on the seabed surrounding *Virginia* have declined since ca. the mid-20th century.
2. Sediment accumulation rates are substantially lower than those of other nearby MRDF studies conducted using the same methods, such as Duxbury et al. (2020) and Keller et al. (2016), where rates are up to ~90% greater [32,41]. Using published models and data, a simple analysis of sediment resuspension potential from waves and currents suggests that annual-scale events can resuspend sediments, likely producing some combination of sediment resuspension, bypass, and possibly erosion that could help produce the low accumulation rates.
3. A volumetric analysis of the lobe combined with Chaytor et al.'s (2020) flow speeds indicates that the *Virginia* lobe is moving at rates sufficient to evacuate the entire *Virginia* lobe volume over timescales of 7–1400 years [8]. If these rates are extrapolated across the entire MRDF and total mass transport is compared to fluvial sediment supply, results suggest that mudflows are moving sediment downslope at mass-transport rates far higher than the rate of annual sediment supply from the Mississippi River.

Funding: This study was funded by the Department of Interior Bureau of Ocean Energy Management, under the cooperative agreements M13AC00013 and M22AC00015, with additional support from the Billy and Ann Harrison Endowment for Sedimentary Geology at Louisiana State University.

Data Availability Statement: Measurements made from collected cores during this study and analysis of data are available from the corresponding author upon reasonable request.

Acknowledgments: The authors would like to thank all those who provided guidance and resources throughout all stages of the project.

Conflicts of Interest: The authors declare no conflict of interest.

References

1. Coleman, J. M., Prior, D. B., & Garrison, L. E. (1978). Submarine landslides in the Mississippi River Delta. All Days. https://doi.org/10.4043/3170-ms
2. Maloney, J. M., Bentley, S. J., Xu, K., Obelcz, J., Georgiou, I. Y., Jafari, N. H., & Miner, M. D. (2020). Mass wasting on the Mississippi River Subaqueous Delta. Earth-Science Reviews, 200, 103001. https://doi.org/10.1016/j.earscirev.2019.103001
3. Bentley, S. J., Keller, G. P., Obelcz, J., Maloney, J. M., Xu, K., Georgiou, I. Y., & Miner, M. D. (2016, December). Cohesive sedimentary processes on river-dominated deltas: New Perspectives from the Mississippi River Delta Front, gulf of mexico. NASA/ADS. https://ui.adsabs.harvard.edu/abs/2016AGUFMEP31C..01B/abstract
4. Maloney, J. M., Bentley, S. J., Xu, K., Obelcz, J., Georgiou, I. Y., & Miner, M. D. (2018). Mississippi River Subaqueous Delta is entering a stage of retrogradation. Marine Geology, 400, 12–23. https://doi.org/10.1016/j.margeo.2018.03.001
5. Bentley S. J., Xu K., Georgiou I. Y., Maloney J. (Baton Rouge, LA: Louisiana State University Coastal Studies Institute). 2022. Mass wasting processes and products of the Mississippi delta front: data synthesis and observation. 158 p. New Orleans (LA): US Dept. of Interior, Bureau of Ocean Energy Management. Cooperative Agreement No.: M13AC00013. OCS Study BOEM 2022-007.
6. Bentley, S.J., Xu, K., Xue, Z.G., Jafari, N., Glaspie, C., et al., 2024. A 21st Century Look at Mass Transport on the Subaqueous Delta of the Mississippi River: OASIS Partnership Preliminary Observations. AGU-ASLO Ocean Sciences Meeting, New Orleans, La.
7. Damour, M., Jones, D., & Chaytor, J. (2021, December). Historic shipwrecks as sentinels for monitoring subsea mudflows on the Mississippi River Delta Front. NASA/ADS. https://ui.adsabs.harvard.edu/abs/2021AGUFMEP41D..04D/abstract
8. Chaytor, J., Baldwin, W. E., Bentley, S. J., Damour, M., Jones, D., Maloney, J., Miner, M., Obelcz, J., & Xu, K. (2020, March 26). Short and long-term movement of mudflows of the Mississippi River Delta Front and their known and potential impacts on oil and gas infrastructure. Geological Society of London Special Publications. Retrieved November 30, 2021
9. Baurick, T, N. O. L. A. | T. T.-P. (2019, February 16). 14-year Taylor Energy oil leak could prove larger than BP spill, new research says. NOLA.com. Retrieved April 25, 2023, from

https://www.nola.com/news/environment/14-year-taylor-energy-oil-leak-could-prove-larger-than-bp-spill-new-research-says/article_c160c6c8-fffd-5cc2-8a13-526978df20e8.html

10. Guidroz, Walter Scott, "Subaqueous, hurricane-initiated shelf failure morpho dynamics along the Mississippi River Delta Front, north-central Gulf of Mexico" (2009). LSU Doctoral Dissertations. 1416. https://digitalcommons.lsu.edu/gradschool_dissertations/1416
11. Obelcz, J., Xu, K., Georgiou, I. Y., Maloney, J., Bentley, S. J., & Miner, M. D. (2017). Sub-decadal submarine landslides are important drivers of deltaic sediment flux: Insights from the Mississippi River Delta Front. Geology. https://doi.org/10.1130/g38688.1
12. Coleman, J. M., Prior, D. B., & Garrison, L. E. (1980). Subaqueous sediment instabilities in the offshore Mississippi River delta (p. 60). Bureau of Land Management, New Orleans OCS Office.
13. Moore, D.G., & Scruton, P.C. (1957). Minor Internal Structures of Some Recent Unconsolidated Sediments. AAPG Bulletin, 41, 2723-2751.
14. Wright, L. D., & Nittrouer, C. A. (1995). Dispersal of river sediments in coastal seas: Six contrasting cases. Estuaries, 18(3), 494. https://doi.org/10.2307/1352367
15. Keen T, Furukawa Y, Bentley S, Slingerland R, Teague W, Dykes J, Rowley C (2006) Geological and oceanographic perspectives on event bed formation during Hurricane Katrina. Geophys Res Lett 33, L23614. doi:10.1029/2006GL027981
16. Walsh JP, Corbett DR, Mallinson D, Goni M, Dail M, Lowey K, Marcinak K, Ryan K, Smith C, Stevens A, Sumners B, Tesh T (2006) Mississippi Delta mudflow activity and 2005 Gulf Hurricanes. EOS Trans Am Geophys Union 87:477–478
17. Xu K, Mickey RC, Chen Q, Harris CK, Hetland RD, Hu K, Wang J (2015) Shelf sediment transport during hurricanes Katrina and Rita. Comput Geosci 90:24–39. doi:10.1016/j.cageo.2015.10.009
18. Denommee K, Bentley S (2013) Influence of mass-transport processes on clinoform mechanics on the southwest Louisiana Shelf. Gulf Coast Assoc Geol Soc Trans 63:205 212
19. Denommee K, Bentley SJ Sr, Harazim D, Macquaker JHS (2016) Hydrodynamic controls on sedimentary fabric development in a shelf clinothem: Southwest Louisiana Continental Shelf. Mar Geol. doi:10.1016/j.margeo.2016.09.013
20. Wright, L. D., Friedrichs, C. T., Kim, S. C., & Scully, M. E. (2001). Effects of ambient currents and waves on gravity-driven sediment transport on continental shelves. Marine Geology, 175(1–4), 25–45. https://doi.org/10.1016/s0025-3227(01)00140-2
21. Macquaker, J. H. S., Bentley, S. J., & Bohacs, K. M. (2010, October 1). Wave-enhanced sediment-gravity flows and mud dispersal across continental shelves: Reappraising sediment transport processes operating in ancient mudstone successions. Geology. https://pubs.geoscienceworld.org/gsa/geology/article/38/10/947/130135/Wave-enhanced-sediment-gravity-flows-and-mud
22. Allison, M. A., Meselhe, E. A., Kleiss, B. A., & Duffy, S. M. (2023). Impact of water loss on sustainability of the Mississippi River channel in its Deltaic Reach. Hydrological Processes. https://doi.org/10.22541/au.167929277.71582944/v1 [Unpublished manuscript]
23. Baldwin, W.E., Ackerman, S.D., Worley, C.R., Danforth, W.W. and Chaytor, J.D. 2018. High-resolution geo-physical data collected along the Mississippi River Delta front offshore of southeastern Louisiana. US Geo-logical Survey Field Activity 2017-003-FA. US Geo- logical Survey data release, https://doi.org/10.5066/F7X929K6
24. Restreppo, G. A. (2019). Deltaic wetland dynamics from seasonal to centennial scales (Order No. 29126715). Available from Dissertations & Theses @ Louisiana State University; ProQuest Dissertations & Theses A&I; ProQuest Dissertations & Theses Global. (2675222694). Retrieved from https://www.proquest.com/dissertations-theses/deltaic-wetland-dynamics-seasonal-centennial/docview/2675222694/se-2
25. Baker, S. R., & Friedman, G. M. (1969). A non-destructive core analysis technique using X-rays. Journal of Sedimentary Research, 39(4), 1371-1383.
26. Cochran, J. K., Masqué, P. (2003). Short-lived U/Th series radionuclides in the ocean: Tracers for scavenging rates, export fluxes and particle dynamics. Uranium-Series Geochemistry, 461–492. https://doi.org/10.1515/9781501509308-016
27. Nittrouer CA, DeMaster DJ, McKee BA, Cutshall NH, Larsen IL (1984) The effect of sediment mixing on Pb-210 accumulation rates for the Washington continental shelf. Mar Geol 54:201–221. doi:10.1016 /0025-3227(84)90038-0
28. Berner, R. A. (1980). Early Diagenesis: A Theoretical Approach. Princeton University Press. https://doi.org/10.2307/j.ctvx8b6p2
29. Aller, R. C. (1980). Quantifying solute distributions in the bioturbated zone of marine sediments by defining an average microenvironment. Geochimica Et Cosmochimica Acta, 44(12), 1955–1965. https://doi.org/10.1016/0016-7037(80)90195-7

30. Nittrouer, C. A., & Sternberg, R. W. (1981). The formation of sedimentary strata in an allochthonous shelf environment: The Washington Continental Shelf. Developments in Sedimentology, 201–232. https://doi.org/10.1016/s0070-4571(08)70300-5
31. Muhammad Z, Bentley SJ, Febo LA, Droxler AW, Dickens GR, Peterson LC, Opdyke BN (2008) Excess 210Pb inventories and fluxes along the continental slope and basins of the Gulf of Papua. J Geophys Res Earth Surf 113:F01S17. doi:10.1029/2006JF000676
32. Keller, G., Bentley, S. J., Georgiou, I. Y., Maloney, J., Miner, M. D., & Xu, K. (2016, October 22). River-plume sedimentation and 210PB/7be seabed delivery on the Mississippi River Delta Front. Geo-Marine Letters. Retrieved November 30, 2021, from https://link.springer.com/article/10.1007/s00367-016-0476-0.
33. Sommerfield, C. K., Nittrouer, C. A., & Alexander, C. R. (1999). 7BE as a tracer of flood sedimentation on the Northern California Continental Margin. Continental Shelf Research, 19(3), 335–361. https://doi.org/10.1016/s0278-4343(98)00090-9
34. Rotondo KA & Bentley SJ (2003) Deposition and resuspension of fluid mud on the western Louisiana inner shelf. Gulf Coast Assoc Geol Soc Trans 53:722–731
35. Bentley, S. J. (2002, January 1). Dispersal of fine sediments from river to shelf: Process and product. AAPG Datapages/Archives. Retrieved October 4, 2022, from https://archives.datapages.com/data/gcags/data/052/052001/1055.htm
36. Galloway, N., Levy, T. and George, T. 2017. Mapping active mudflow features off Southwest Pass, Louisiana, Gulf of Mexico. Presented at Hydrographic Society of America 2017 Annual Meeting, 20–23 March, Galveston, TX, http://ushydro2019.thsoa.org/wp-content/uploads/2017/04/Galloway_Hydro2017_MappingMudflowFeatures-1.pdf
37. Bentley, S. J., & Nittrouer, C. A. (2003). Emplacement, modification, and preservation of event strata on a flood-dominated continental shelf: Eel shelf, Northern California. Continental Shelf Research, 23(16), 1465-1493. https://doi.org/10.1016/j.csr.2003.08.005
38. Wheatcroft, R. A., Wiberg, P. L., Alexander, C. R., Bentley, S. J., Drake, D. E., Harris, C. K., & Ogston, A. S. (2007). Post-depositional alteration and preservation of sedimentary strata. Continental Margin Sedimentation, 101–155. https://doi.org/10.1002/9781444304398.ch3
39. Bentley, S.J., Sheremet, A., and Jaeger, J.M., 2006, Preservation potential of event layers on continental shelves: a model and observations. Continental Shelf Research 26: 2108-2124.
40. Bentley, S. J., Blum, M. D., Maloney, J., Pond, L., & Paulsell, R. (2016). The Mississippi River Source-to-sink system: Perspectives on tectonic, climatic, and anthropogenic influences, miocene to anthropocene. *Earth-Science Reviews*, *153*, 139–174. https://doi.org/10.1016/j.earscirev.2015.11.001
41. Duxbury, J., Bentley, S.J., Xu, K. (2023). Temporal scales of mass wasting sedimentation across the Mississippi River Delta Front delineated by 210Pb/137Cs Geochronology [Unpublished manuscript]
42. Lo, E.L., Bentley, S.J., & Xu, K. Experimental study of cohesive sediment consolidation and resuspension identifies approaches for coastal restoration: Lake Lery, Louisiana. Geo-Mar Lett 34, 499–509 (2014). https://doi.org/10.1007/s00367-014-0381-3
43. Sha, X., Xu, K., Bentley, S. J., & Robichaux, P. A. (2018). Characterization and modeling of sediment settling, consolidation, and suspension to optimize coastal Louisiana Restoration. Estuarine, Coastal and Shelf Science, 203, 137–147. https://doi.org/10.1016/j.ecss.2018.02.008
44. Xu, K.H., Corbett, D., Walsh, J., Young, D., Briggs, K., Cartwright, G., Friedrichs, C., Harris, C., Mickey*, R., Mitra, S., 2014. Seabed Erodibility Variations on the Louisiana Continental Shelf Before and After the 2011 Mississippi River Flood, Estuarine, Coastal and Shelf Science, 149, 283-293. http://dx.doi.org/10.1016/j.ecss.2014.09.002.
45. Xu, K.H., Harris, C.K., Hetland, R.D., Kaihatu, J. M., 2011. Dispersal of Mississippi and Atchafalaya Sediment on the Texas-Louisiana Shelf: Model Estimates for the Year 1993, Continental Shelf Research, 31, 1558-1575. doi:10.1016/j.csr.2011.05.008.
46. Zang, Zhengchen, George Xue, Kehui Xu, Samuel J Bentley, Qin Chen, Eurico J D'Sa, Qian Ge, 2019, A Two Decadal (1993–2012) Numerical Assessment of Sediment Dynamics in the Northern Gulf of Mexico, Water https://doi.org/10.3390/w11050938
47. Whitehouse, R., Soulsby, R., Roberts, W., Mitchener, H., (2000). Dynamics of estuarine muds: A manual for practical applications. Telford.

48. Allison, M. A., Demas, C. R., Ebersole, B. A., Kleiss, B. A., Little, C. D., Meselhe, E. A., Powell, N. J., Pratt, T. C., & Vosburg, B. M. (2012). A water and sediment budget for the lower Mississippi–Atchafalaya river in Flood Years 2008–2010: Implications for sediment discharge to the oceans and coastal restoration in Louisiana. Journal of Hydrology, 432-433, 84–97. https://doi.org/10.1016/j.jhydrol.2012.02.020
49. Bureau of Ocean Energy Management. (2023, November 11). Pipelines. Geographic mapping data in digital format. https://www.data.boem.gov/Main/Mapping.aspx